

# Whole Arm Planning for a Soft and Highly Compliant 2D Robotic Manipulator

Andrew D. Marchese, Robert K. Katzschmann, and Daniela Rus

**Abstract**—Soft continuum manipulators have the advantage of being more compliant and having more degrees of freedom than rigid redundant manipulators. This attribute should allow soft manipulators to autonomously execute highly dexterous tasks. However, current approaches to motion planning, inverse kinematics, and even design limit the capacity of soft manipulators to take full advantage of their inherent compliance. We provide a computational approach to whole arm planning for a soft planar manipulator that advances the arm’s end effector pose in task space while simultaneously considering the arm’s entire envelope in proximity to a confined environment. The algorithm solves a series of constrained optimization problems to determine locally optimal inverse kinematics. Due to inherent limitations in modeling the kinematics of a highly compliant soft robot and the local optimality of the planner’s solutions, we also rely on the increased softness of our newly designed manipulator to accomplish the whole arm task, namely the arm’s ability to harmlessly collide with the environment. We detail the design and fabrication of the new modular manipulator as well as the planner’s central algorithm. We experimentally validate our approach by showing that the robotic system is capable of autonomously advancing the soft arm through a pipe-like environment in order to reach distinct goal states.

## I. INTRODUCTION

Soft robots are predominantly made of soft materials and have a continuously deformable structure, providing a relatively large number of degrees of freedom when compared to their hard counterparts, as reviewed by Trivedi, Rahn, Kier, and Walker [1]. Furthermore, soft robots are often characterized by distributed actuation and are fundamentally underactuated, that is they have many passive degrees of freedom. As a soft robot’s body becomes more compliant, its dexterity increases and this is a major advantage over traditional hard bodied robots. For example, such a dexterous robot can access confined areas and execute economically difficult tasks. However, to actually get this benefit from soft robots, we need both computational advances in kinematics and control, as well as advanced designs and fabrication techniques for soft manipulators. Traditional approaches to kinematics and control for soft robots do often not consider the robot’s entire shape or envelope, preventing autonomous navigation in confined environments.

In this work, we provide an approach for autonomously moving a soft and highly compliant planar robot arm through a confined environment. We provide a computational approach to whole arm planning that finds a solution to the inverse kinematics problem for this class of arms. The solution

Andrew D. Marchese, Robert K. Katzschmann, and Daniela Rus are with the Computer Science and Artificial Intelligence Laboratory, Massachusetts Institute of Technology, 32 Vassar St. Cambridge, MA 02139, USA, {andy, rkk, rus}@csail.mit.edu

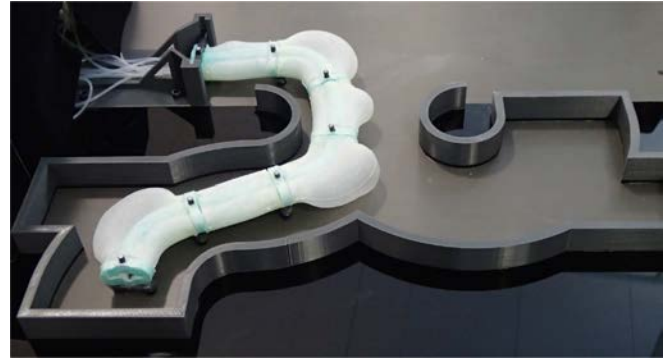


Fig. 1. Entirely soft planar manipulator using whole arm planning to move its entire body through a confined pipe-like environment.

considers both the task of advancing the arm’s end effector pose as well as the whole arm’s changing envelope in relation to the environment. We find a transformation from the arm’s task space to its arc space that is aware of the soft arm’s entire shape. In the planar case, the task space is the position and orientation of points along the robot, whereas the arc space consists of the independent body segment curvatures and lengths. Specifically, we pose a series of constrained nonlinear optimization problems solving for locally optimal arc space parameters which minimize the robot’s collisions with its environment while tracking a user-specified path for the manipulator’s end effector. A key feature of our approach is that we do not prevent collisions, but rather minimize their likelihood. In fact, since we have designed an entirely soft and compliant robot, we can use collisions to assist us in accomplishing the task.

We describe the design of an *entirely* soft and highly compliant continuum manipulator, composed of 100% soft silicone rubber, which improves our previous work [2] in several ways. This arm design draws inspiration from soft pneumatic tentacles developed by Martinez et al. [3]. The arm is composed of multiple modular body segments, each capable of bi-directional bending using only two lateral fluidic elastomer channels. We exclude an inextensible but continuously deformable backbone and replace this with an extensible rubber layer and hollow core. Lastly, we develop a fabrication process for these body segments that does not require lamination, making the design robust to separation at high pressures.

Despite variability in the design of soft continuum robots [4] [5] [6] [7] [8] [9] [10] [11], their kinematics are often represented using a piece-wise constant curvature model.

The piece-wise constant curvature assumption means each body segment of a multi-segment arm is assumed to deform with constant curvature. This representation for continuum robots is reviewed by Webster and Jones [12]. Hannan and Walker [13] provide an early example of the piecewise constant curvature model. As Webster’s review discusses, the generality of this modeling assumption is due to the physics behind the deformation. Specifically, Gravagne, Rahn, and Walker [14] and Li and Rahn [15] show a moment applied by a guided cable fixed to the end of a continuum backbone produces constant curvature along the backbone. Jones and Walker [16] show that the constant curvature concept also applies to pneumatic muscle actuators bending a continuum backbone. Recently, Onal, Chen, Whitesides, and Rus show rectangular fluidic elastomer actuators with uniform channels deform along an arc of constant curvature [17]. Marchese, Komorowski, Onal and Rus [2] demonstrate autonomous closed-loop positioning of a soft and highly compliant inextensible planar arm under the piecewise constant curvature modeling assumption. Both the forward kinematics and the closed-loop curvature controller of that work are reused for the new extensible soft planar arm presented in this paper.

A limitation of existing approaches to solving the inverse kinematics problem for soft continuum arms is that currently the whole arm, in addition to the end effector’s pose, is not considered in the solution. Autonomous obstacle avoidance and movement through a confined environment is difficult without a computational solution to the inverse kinematics problem that is aware of the robot’s whole arm in space. Buckingham [18] articulates as a distinguishing advantage of a snake-like arm, that it can potentially achieve the primary task of tip control, while meeting the secondary task of shaping the whole arm. Neppalli, Csencsits, Jones, and Walker [19] provide a closed-form IK solution for continuum arms, but the Jacobian-based solution only considers the endpoint of the final body segment and obstacle avoidance requires manual planning. Jones and Walker [20] control Air-OCTOR and OctArm using fast real-time Jacobian control over task-space, but rely on joystick control for whole arm tasks like manipulation and grasping [21]. Local optimization has shown promising results for rigid-bodied redundant manipulators [22], but as far as we are aware such a technique has not been used to solve the whole body manipulation problem for a soft robot. Furthermore, we are not aware of any existing soft-bodied fluidic robots with highly deformable exterior envelopes [23] [17] [24] [25] [2] [26] [27] [3] that consider whole body manipulation when moving in task-space. With fewer kinematic constraints, the envelop of these soft robots expand or radially bulge at locations along the body under actuation. Accordingly, whole body planning for soft and highly compliant robots must take into consideration this dynamic envelope.

The main contributions of this paper to soft-bodied robotics are:

- A planner for whole body motion of a soft planar manipulator that considers the tasks of both controlling end effector pose while minimizing collisions between

the whole arm’s changing envelop and a confining environment.

- A modular design for a pneumatic highly compliant planar manipulator that is composed entirely of soft silicone rubber, which improves on [2].

## II. DESIGN

The arm for planar manipulation is made from modular segments entirely composed of soft silicone rubber. Each segment is capable of bending bidirectionally, has two concentric layers of rubber, a hollow inner core, and distributed pneumatic actuators. This design draws inspiration from the soft rubber tentacles developed by Martinez et al. [3] which use embedded PneuNet actuators in a similar two layer construction. Figure 2 details the design of an individual arm segment. Here, the outer layer is made of a very soft silicone

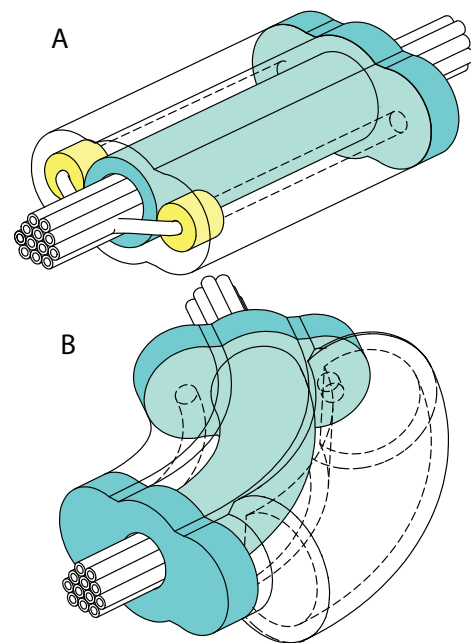


Fig. 2. One of the modular body segments composing the entirely soft planar pneumatic arm. Panel A depicts the segment in an unactuated state. Here, the segment’s outer layer of soft silicone rubber is shown as a transparent outline, the slightly stiffer silicone inner layer is shown in cyan, crush resistant silicon inlets to the embedded expanding pneumatic channels are shown in yellow, and the internal tubing bundle is shown in white. Panel B shows the body segment in an actuated or curved state and the expansion of the pressurized channel is schematically represented.

rubber shown as *transparent* and the inner layer is made of slightly stiffer silicone rubber shown in *cyan*. As panel B details, bidirectional bending is achieved by pneumatically pressurizing either of two laterally embedded cylindrical channels within the softer outer layer. When pressurized, the channel undergoes high strain and effectively lengthens. Because of the partially constraining inner layer, this expansion generates curvature about the stiffer but extensible center. The segment has rubber endplates which allow multiple segments to be concatenated end-to-end forming the multi-segment manipulator shown in Figure 1. Additionally, the hollow inner core enables a bundle of soft silicone tubes

shown in *white* to pass through each segment. On one end, each tube individually connects to each actuated channel in the multi-segment arm by means of a crush resistant silicone insert shown in *yellow*. On the other end, each tube connects to the outlet of a fluidic drive cylinder detailed in [2]. These cylinders allow each channel to be individually pressurized. The relationship between neutral axis curvature, internal channel pressure, and delivered volume for a single arm segment is characterized in Figure 3. In this experimental characterization, one of the segment's two channels was incrementally filled under volume control and both internal channel pressure and curvature were derived from measurements at each fill increment. Curvature is assumed to be constant along the length of the segment and is uniquely defined by measuring the starting pose and end point of the segment.

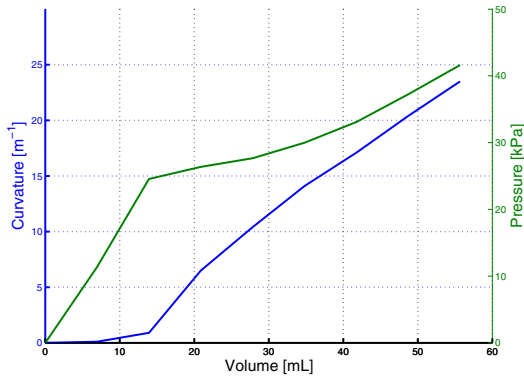


Fig. 3. Experimental characterization of a single soft arm segment. Volume is incrementally delivered to one of the segment's embedded channels and both the resulting internal pressure and segment curvature are derived from measurements.

This design is an extension of the planar manipulator presented in [2] in that we change both its kinematic constraints and distributed actuators. We remove the inextensible constraining backbone layer and replace this with an extensible, but partially constraining silicone layer. Also, we move away from the multiple vertical channels characterizing fluidic elastomer actuators [23] and adopt two lateral cylindrical-shaped channels. The primary benefits of this new design compared to the previous design are that (1) its entirely soft construction, concentric layers, and hollow core make this arm simpler to fabricate, (2) the modular design enables scalability in the number of body segments, and (3) the actuators do not have the problem of delaminating under high pressures, because the embedded channels are not at the interface between layers.

### III. FABRICATION

In the following section we describe the fabrication process for this robot as well as the tools and equipment used, which are listed in Table I. We fabricate the arm through a casting process that uses pourable silicone rubber<sup>2,4</sup> and 3D printed molds<sup>1</sup>.

Figure 4 details this process. First, each body segment is independently fabricated in steps 1-3 and later these segments are joined serially to form the arm in steps 4 and 5. To start, a four piece mold was printed. The mold is poured in two steps. In step 1, a low elastic modulus rubber<sup>2</sup> is mixed, degassed in a vacuum<sup>3</sup>, and poured to form the body segment's soft outer layer shown in *white*. The mold's outer piece, one half of it is shown in *green*, functions to form the segment's exterior. Metal rods shown in *pink* are inserted into the mold and are held in place by the *orange* bottom piece of the mold. These rods will form the cavities for the segment's two lateral pneumatic actuation channels.

After the outer layer has cured, the *red* rigid sleeve is removed in step 2 from the extruded feature of the *orange* bottom piece of the mold. This produces a cavity into which the slightly stiffer rubber<sup>4</sup> is poured, forming the segment's partially constraining inner layer shown in *cyan*. The extruded feature of the *orange* bottom piece, shown by its *orange* end tip, functions to produce the segment's hollow interior core.

In step 3, the body segments are removed from their molds and joined to soft rubber<sup>4</sup> endplates shown in *cyan* using adhesive<sup>5</sup>. The small *yellow* channel inlets were added on one side of the *pink* metal pins during step 1.

In step 4, soft silicone tubes<sup>6</sup> are joined to each embedded channel's inlet. The resulting bundle of tubes is passed through each segment's hollow interior. Lastly, in step 5 multiple body segments are attached at their endplates using the same adhesive<sup>5</sup>.

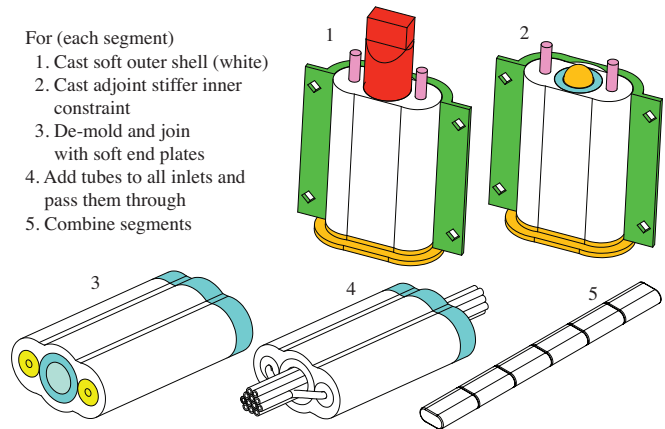


Fig. 4. Each body segment is cast using a two step process where the outer soft layer (1) and inner stiffer layer (2) are poured. Once cured, the segments are joined to endplates using silicone adhesive (3). Next, silicone tubing is connected to each embedded channel and the resulting tubing bundle is run inside each segment's hollow interior (4). Lastly, the body segments are serially connected using adhesive to form the manipulator (5).

### IV. CONTROL

The key operation for controlling the arm is closed-loop curvature control. By controlling the curvatures of the arm segments, we can achieve forward and inverse kinematics as shown in [2]. Here we extend on this work to derive a planning system for planar soft arms. The planning and

TABLE I  
COMMERCIALY AVAILABLE TOOLS AND EQUIPMENT

1	Fortus 400mc, Stratasys Ltd., Eden Prairie, MN
2	Ecoflex 0030, Smooth-On, Easton, PA
3	AL Cube, Abbess Instruments and Systems, Inc., Holliston, MA
4	Mold Star 15, Smooth-On, Easton, PA
5	Silicone Sealant 732, Dow Corning Corp, Midland, MI
6	PN 51845K52, McMaster, Princeton, NJ

inverse kinematics problems are solved simultaneously using constrained nonlinear optimization as opposed to an iterative jacobian approach.

#### A. Kinematics

The orientation of any point  $s \in [0, L_i]$  along the arc representing segment  $i$  within  $n$  arm segments can be expressed as:

$$\theta_i(s) = k_i s + \theta_i(0) \quad (1)$$

where  $k_i$  is the given curvature of element  $i$ . The serial connection of the segments leads to  $\theta_i(0) = \theta_{i-1}(L_{i-1})$ . The forward kinematics at arc length  $s$  on segment  $i$  along the arm's central axis can therefore be expressed as:

$$x_i(s) = x_{i-1}(L_{i-1}) + \int_0^s \cos(\theta_i(s')) ds', \quad (2)$$

$$y_i(s) = y_{i-1}(L_{i-1}) + \int_0^s \sin(\theta_i(s')) ds'. \quad (3)$$

whereas  $x_i(s)$  and  $y_i(s)$  are cartesian coordinates, and  $L_i$  is the given length of segment  $i$ .

#### B. Curvature Control

The control of the new arm design is achieved by the use of the previously developed system for closed-loop curvature control of each segment [2]. In short, this closed-loop curvature controller periodically receives discrepancies between the soft arm's measured and requested curvatures  $k_i$  and uses a two-staged cascaded control approach to adjust the fluidic drive cylinders and resolve the error. An external tracking system (Opti Track, NaturalPoint Inc., Corvallis, OR) detects markers positioned at the end of each arm segment and calculates the measured curvatures of each segment using the arm's inverse kinematics. The measured curvatures minus the reference curvatures result in errors, which are passed on to PI controllers also running at 20 Hz. The outputs of the PI controllers are used as set points for the embedded PID controllers of the linear actuators. These controllers run at 1 kHz and ensure that the actuated cylinder pistons provide the appropriate volumetric displacement in order to attain the desired curvatures.

#### C. Whole Arm Planner

We are controlling the shape of a soft planar multi-segment continuum arm to move into a bounded environment. We represent the arm using a piecewise constant curvature model. That is, each of the arm's  $n$  body segments have length  $l_i$  and are assumed to deform in an arc of constant curvature

$\kappa_i$ , where  $i = 1 \dots n$ . The task space of the arm consists of the position and orientation of a point  $w = [x, y, \theta]$  along the arm. The goal of this algorithm is to find a local optimum for the transformation from the arm's task space to the arm's configuration space [12] described by curvature values while considering the robot's envelope points  $h \in H \subseteq \mathbb{R}^2$  in relation to its environment points  $e \in E \subseteq \mathbb{R}^2$ . The envelope  $H$  is modeled by trapezoids scaled linearly according to the measured curvature value. The environment  $E$  is represented as a set of points and is known *a priori*. We assume that the arm is initially always placed in a free space outside the bounded environment we want to enter. Also, a series of task space waypoints is predefined by the user, where the first waypoint is placed at the inlet to the environment. All following waypoints describe a path that would lead to a final goal position inside the environment.

The optimization approach to solve for whole arm control is laid out in Algorithm 1, visually supported by Figure 5 and explained in further detail in the following. At the start time  $t = 1$ , we set the arm segments to a locally optimal  $\kappa$ , that places the tip according to the forward kinematics  $\text{FORWKIN}(\kappa, l)$  at the first waypoint  $w_1$  while ensuring that the extreme curvatures  $\kappa_{min}$  and  $\kappa_{max}$  are not exceeded. The extreme curvatures are experimentally determined to be either the maximum curvatures achievable given the fixed volumetric displacements of the fluidic drive cylinders or curvatures which damage the segments due to over inflation.

After the start, we enter a loop until the last waypoint at time step  $N$  is reached. At the start of the loop, we find the closest environment points left  $e_{1,t}$  and right  $e_{1,t}$  of the arm's body shape. To define the two sides of the arm, we use the arm's approach vector  $n_t$  and the angle  $\alpha = \angle(e - w_t, n_t)$ . The origin of the end-effector's approach vector  $n_t$  is defined by the positions  $x$  and  $y$  and its direction by the angle  $\theta$ . Positive values for  $\alpha$  result in the closest point  $e_{1,t}$  left of  $w_t$  and negative values result in  $e_{2,t}$  to the right of  $w_t$ . Next, we calculate the arm hulls  $\text{ARMHULL}(\kappa_t, L)$  of both sides by modeling each segments bulging side with a trapezoid that is linearly scaled in height by the curvature value. The concave side is not vacuumed during the actuation process, so the hull is described by a constant offset from the curved body centerline. For every stored environment point  $e_{i,j}$ ,  $i = 1 \dots 2$  and  $j = 1 \dots t$ , we find the closest hull points, calculate their connection vector and calculate the normals of the environment  $\text{ENVNORMAL}(e_{i,j})$  at each stored environment point. We then perform an optimization to find the curvatures that best fit the hull into the environment while achieving the current target waypoint. Finally, the time step is incremented and the loop repeats until the last waypoint is calculated.

#### D. Implementation

The optimization algorithm was implemented using Matlab's Optimization Toolbox with the function calls *fmincon*, which finds the minimum of a constrained nonlinear multivariable function. Sequential Quadratic Programming was used as the solver with a relative upper bound of  $2 \times 10^{-3}$

---

**Algorithm 1** Whole Arm Planner Algorithm Outline
 

---

**Parameters:** environment  $E \subseteq \mathbb{R}^2$ , segment lengths  $\ell \subseteq \mathbb{R}^n$ 

```

1  $t \leftarrow 1$  // set first time step to 1
2  $\kappa_t \leftarrow \min_{\kappa} \{ \kappa \cdot \kappa \}$  s.t.  $w_t - f = \mathbf{0}$ ,  $\kappa_{min} \leq \kappa \leq \kappa_{max}$ 
   where  $f = \text{FORWKIN}(\kappa, \ell)$  // local opt. for initial curvatures
3 while  $t \leq N$  do // loop until last waypoint  $N$  reached
4    $E_1 \leftarrow E \mid \sin(\alpha) > 0$  // environment to the left of the arm hull
5    $e_{1,t} \leftarrow \operatorname{argmin}_{e \in E_1} \{ \|e - w_t\| \}$ 
6    $E_2 \leftarrow E \setminus E_1$  // environment to the right of the arm hull
7    $e_{2,t} \leftarrow \operatorname{argmin}_{e \in E_2} \{ \|e - w_t\| \}$ 
8    $(H_1, H_2) \leftarrow \text{ARMHULL}(\kappa_t, \ell)$  // left and right hull points
9   for  $j = 1 \dots t$  do // for all times until t
10    for  $i = 1 \dots 2$  do // for left and right
11       $h_{i,j} \leftarrow \operatorname{argmin}_{h \in H_k} \{ \|e_{i,j} - h\| \}$  // closest hull points
12       $b_{i,j} = e_{i,j} - h_{i,j}$  // vector betw. hull and environment
13       $a_{i,j} = \text{ENVNORMAL}(e_{i,j})$  // normal to wall
14       $\kappa_t \leftarrow \max_{\kappa} \left\{ \sum_{j=1}^t \sum_{i=1}^2 \|b_{i,j}\| \ln(a_{i,j} \cdot b_{i,j} + 1) \right\}$ 
        s.t.  $w_t - f = \mathbf{0}$ ,  $\kappa_{min} \leq \kappa \leq \kappa_{max}$ 
        where  $f = \text{FORWKIN}(\kappa, \ell)$ 
15     $t \leftarrow t + 1$ 

```

---

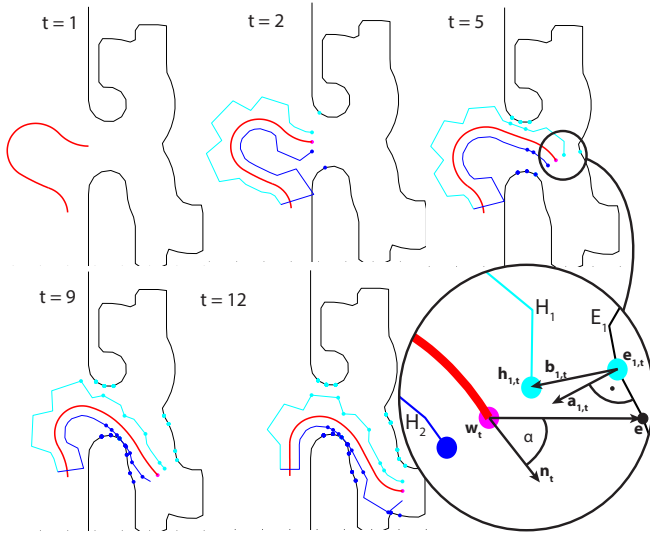


Fig. 5. Whole Arm Planner: The soft robot is depicted for several time steps  $t$  by a red body center line, a cyan line for the left body shape and a blue line for the right body shape. The black line depicts the bounded environment. The purple dot at the end of the red center line represents the end-effector of the arm. At every time step  $t$ , the end-effector reaches the planned waypoint through the control by the previously published curvature controller [2]. At timestep  $t = N = 12$ , the last point inside the bounded environment is reached. A close-up view shows the vectors relevant for the whole body planner described in Subsection IV-C and Algorithm 1.

on the magnitude of the constraint functions. The maximal function evaluations were bounded by 2000 and the lower bound on the size of a step was given by  $1 \times 10^{-6}$ . The function *dsearch* was used to find the minimal distant points on the environment and on the hull.

## V. RESULTS

To experimentally validate the soft robot's ability to successfully advance through a confined environment, we carry out a series of experiments using a six segment soft planar manipulator. The primary goal of these experiments is to see if the whole body planner outlined in the controls section can incrementally advance the robot's end effector pose according to a series of user-specified waypoints, ultimately terminating at the end of one of four distinct pipe-like sections. To achieve this primary goal, the planner also has to successfully accomplish the intermediate task of conforming the whole arm's shape to the pipe-like environment. The purpose of these experiments is to show that through a combination of computation (i.e., the whole body planning algorithm) and design (i.e., the inherent softness and compliance of the manipulator), we can successfully accomplish the primary task. If we ignore the arm's softness and high compliance, the planar arm provides only 6 degrees of freedom (1 degree of freedom per segment) and the primary task constrains 3 degrees of freedom (X-Y position and orientation). In the non-compliant case, this would leave only 3 degrees of freedom for the whole body planner to conform the arm's whole body to the environment's interior at any point along the waypoint path. Fortunately, the compliance of the arm provides many passive degrees of freedom and we leverage this by making occasional, almost frictionless contacts with the rigid environment. Again, the computational solution does not prevent collisions, but simply minimizes their likelihood and magnitude. With a rigid manipulator, these collisions may be harmful, but with an entirely soft and highly compliant robot these collisions are harmless and when combined with our planner, enable the robot to accomplish the task.

Specifically, a rigid pipe-like environment using 3D printed walls is presented in these experiments. To create frictionless collisions, we coat the exterior of the robot with a thin layer of talc powder, reducing the friction between the robot and the wall. In order to constrain the robot's motion to the X-Y plane, reduce friction between the robot and the ground, and prevent segment torsion about the hollow core, small ball transfers are placed underneath each segment's soft endplate.

Before the robot autonomously snakes through the environment, it is reset to an initial near-zero curvature outside the confined environment; see Figure 6 A. Independent of the experiment's targeted final waypoint, the planner finds the same solution to maneuver the arm to the pipe-like environment's entrance. This solution is shown in B. As the planner autonomously advances the arm's end effector through the environment's center and considers the proximity of the changing envelope to the boundaries, collisions

inevitably happen and are highlighted in red at C. The arm successfully reaches one of four goal states depicted in D-F. Table II contains data for several successful demonstrations of the arm advancing through the environment to the end goal poses. Approximately 12 waypoints were used along each path.  $T_{solve}$  is the average time the planner took to compute a solution at a given path waypoint in simulation.  $P_{error}$  and  $O_{error}$  are the position and orientation errors between the manipulator's end effector and the goal pose.  $T_{task}$  is the time the manipulator took to advance from the starting location to the goal pose. We have also indicated the number of collisions between the manipulator and the environment for several of these trials. Of 30 path attempts 24 resulted in successful advances to goal locations and 6 were unsuccessful. The typical failure scenario was the manipulator becoming lodged in the environment due to excessive contact friction.

The speed of the manipulator advancing along the path is limited by how quickly the target curvatures determined by the algorithm are realized by the physical system. In the ideal case, the system would realize target curvatures as fast as the algorithm computes them; however, because of the increased compliance of the manipulator and the control approach outlined in [2], the algorithm must halt until the physical system can catch up. In order to improve the speed of the given physical system, the control policy could be optimized by also considering the arm's dynamics as constraints.

TABLE II  
EXPERIMENTAL VALIDATION

Goal #	$T_{solve}$ (sec)	Trial #	$P_{error}$ (cm)	$O_{error}$ (deg)	$T_{task}$ (sec)	Collisions #
1	0.9	1	0.9	10.4	44	
		2	0.5	0.1	54	
		3	1.3	1.6	55	6
		4	0.7	1.3	50	4
		5	0.4	0.3	50	2
2	0.9	1	0.7	2.7	44	
		2	0.3	0.6	53	
		3	0.4	0.6	53	4
		4	1.1	5.3	53	2
		5	1.2	4.9	55	3
3	1.0	1	3.1	2.1	42	
		2	3.5	2.5	44	
		3	2.8	0.6	50	8
		4	2.4	4.5	49	6
		5	3.6	3.0	48	12
		6	1.3	1.7	50	
		7	3.5	8.7	52	7
		8	3.4	6.0	53	8
		9	3.4	4.9	50	8
4	1.1	1	4.1	10.7	60	
		2	5.1	17.5	48	4
		3	8.0	25.3	47	12
		4	6.1	21.4	48	7
		5	5.6	17.1	50	6
		6	4.4	14.7	53	13

## VI. CONCLUSION

We addressed the problem of maneuvering a soft planar manipulator through a confined environment. To achieve this,

we presented an entirely soft and modular manipulator design combined with a whole arm planar planning algorithm that considers the robots changing envelope. We demonstrated the ability of an entirely soft manipulator to autonomously maneuver through a pipe-like environment, which leads to many potential applications. In a manufacturing setting, this could resemble a soft robot executing tasks requiring high dexterity when handling delicate objects. In a human-centric environment, whole arm manipulation may enable soft robots to interact safely with humans. Furthermore, in a surgical setting, highly compliant soft robots under whole body control may assist with operations in sensitive environments.

## ACKNOWLEDGMENT

The support by Mikhail Volkov is highly appreciated. This work was done in the Distributed Robotics Laboratory at MIT with support from the National Science Foundation, grant numbers NSF IIS1226883 and NSF CCF1138967, and National Science Foundation Graduate Research Fellowship Program, primary award number 1122374. We are grateful for this support. The authors declare no competing financial interests.

## REFERENCES

- [1] D. Trivedi, C. D. Rahn, W. M. Kier, and I. D. Walker, "Soft robotics: Biological inspiration, state of the art, and future research," *Applied Bionics and Biomechanics*, vol. 5, no. 3, pp. 99–117, 2008.
- [2] A. D. Marchese, K. Komorowski, C. D. Onal, and D. Rus, "Design and control of a soft and continuously deformable 2d robotic manipulation system," in *Proceedings of IEEE International Conference on Robotics and Automation*, 2014.
- [3] R. V. Martinez, J. L. Branch, C. R. Fish, L. Jin, R. F. Shepherd, R. Nunes, Z. Suo, and G. M. Whitesides, "Robotic tentacles with three-dimensional mobility based on flexible elastomers," *Advanced Materials*, vol. 25, no. 2, pp. 205–212, 2013.
- [4] I. A. Gravagne and I. D. Walker, "Uniform regulation of a multi-section continuum manipulator," in *Robotics and Automation, 2002. Proceedings. ICRA'02. IEEE International Conference on*, vol. 2. IEEE, 2002, pp. 1519–1524.
- [5] M. B. Pritts and C. D. Rahn, "Design of an artificial muscle continuum robot," in *Robotics and Automation, 2004. Proceedings. ICRA'04. 2004 IEEE International Conference on*, vol. 5. IEEE, 2004, pp. 4742–4746.
- [6] W. McMahan, B. A. Jones, and I. D. Walker, "Design and implementation of a multi-section continuum robot: Air-octor," in *Intelligent Robots and Systems, 2005.(IROS 2005). 2005 IEEE/RSJ International Conference on*. IEEE, 2005, pp. 2578–2585.
- [7] W. McMahan, V. Chitrakaran, M. Csencsits, D. Dawson, I. D. Walker, B. A. Jones, M. Pritts, D. Dienno, M. Grissom, and C. D. Rahn, "Field trials and testing of the octarm continuum manipulator," in *Robotics and Automation, 2006. ICRA 2006. Proceedings 2006 IEEE International Conference on*. IEEE, 2006, pp. 2336–2341.
- [8] G. Chen, M. T. Pham, and T. Redarce, "Development and kinematic analysis of a silicone-rubber bending tip for colonoscopy," in *Intelligent Robots and Systems, 2006 IEEE/RSJ International Conference on*, 2006, pp. 168–173.
- [9] D. B. Camarillo, C. R. Carlson, and J. K. Salisbury, "Configuration tracking for continuum manipulators with coupled tendon drive," *Robotics, IEEE Transactions on*, vol. 25, no. 4, pp. 798–808, 2009.
- [10] R. Kang, D. T. Branson, T. Zheng, E. Guglielmino, and D. G. Caldwell, "Design, modeling and control of a pneumatically actuated manipulator inspired by biological continuum structures," *Bioinspiration & biomimetics*, vol. 8, no. 3, p. 036008, 2013.
- [11] H. Wang, W. Chen, X. Yu, T. Deng, X. Wang, and R. Pfeifer, "Visual servo control of cable-driven soft robotic manipulator," in *Intelligent Robots and Systems (IROS), 2013 IEEE/RSJ International Conference on*, Nov 2013, pp. 57–62.

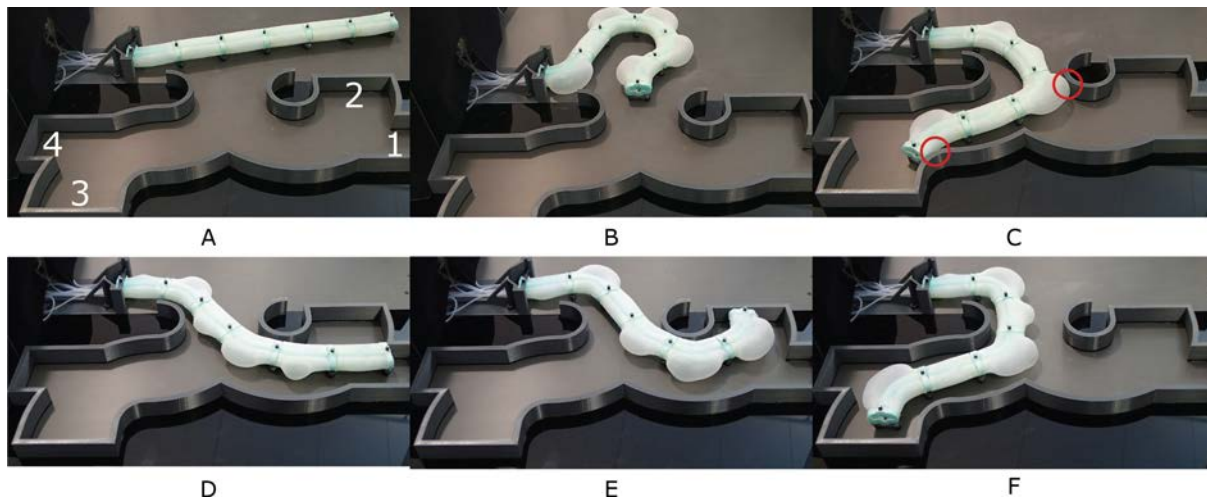


Fig. 6. Experimental validation of the soft robot's ability to autonomously navigate through a confined environment. A shows the starting point of the robot and the positions of the goal locations, 1-4. B depicts the arm advancing to the entrance of the environment. C illustrates the ability of the soft robot to collide with the boundaries of the environment. Lastly, D-F depict final goal points 1-3 respectively, goal point 4 is in the pipe section closest to the manipulator's base (not shown).

- [12] R. J. Webster and B. A. Jones, "Design and kinematic modeling of constant curvature continuum robots: A review," *The International Journal of Robotics Research*, vol. 29, no. 13, pp. 1661–1683, 2010.
- [13] M. W. Hannan and I. D. Walker, "Kinematics and the implementation of an elephant's trunk manipulator and other continuum style robots," *Journal of Robotic Systems*, vol. 20, no. 2, pp. 45–63, 2003.
- [14] I. A. Gravagne, C. D. Rahn, and I. D. Walker, "Large deflection dynamics and control for planar continuum robots," *Mechatronics, IEEE/ASME Transactions on*, vol. 8, no. 2, pp. 299–307, 2003.
- [15] C. Li and C. D. Rahn, "Design of continuous backbone, cable-driven robots," *Journal of Mechanical Design*, vol. 124, p. 265, 2002.
- [16] B. A. Jones and I. D. Walker, "Practical kinematics for real-time implementation of continuum robots," *Robotics, IEEE Transactions on*, vol. 22, no. 6, pp. 1087–1099, 2006.
- [17] C. D. Onal, X. Chen, G. M. Whitesides, and D. Rus, "Soft mobile robots with on-board chemical pressure generation," in *International Symposium on Robotics Research, ISRR*, 2011.
- [18] R. Buckingham, "Snake arm robots," *Industrial Robot: An International Journal*, vol. 29, no. 3, pp. 242–245, 2002.
- [19] S. Neppalli, M. A. Csencsits, B. A. Jones, and I. D. Walker, "Closed-form inverse kinematics for continuum manipulators," *Advanced Robotics*, vol. 23, no. 15, pp. 2077–2091, 2009.
- [20] B. A. Jones and I. D. Walker, "Kinematics for multisection continuum robots," *Robotics, IEEE Transactions on*, vol. 22, no. 1, pp. 43–55, 2006.
- [21] M. Csencsits, B. A. Jones, W. McMahan, V. Iyengar, and I. D. Walker, "User interfaces for continuum robot arms," in *Intelligent Robots and Systems, 2005.(IROS 2005), 2005 IEEE/RSJ International Conference on*. IEEE, 2005, pp. 3123–3130.
- [22] D. N. Nenchev, "Redundancy resolution through local optimization: A review," *Journal of Robotic Systems*, vol. 6, no. 6, pp. 769–798, 1989.
- [23] N. Correll, C. D. Onal, H. Liang, E. Schoenfeld, and D. Rus, "Soft autonomous materials using active elasticity and embedded distributed computation," in *12th International Symposium on Experimental Robotics. New Delhi, India*, 2010.
- [24] C. D. Onal and D. Rus, "Autonomous undulatory serpentine locomotion utilizing body dynamics of a fluidic soft robot," *Bioinspiration & biomimetics*, vol. 8, no. 2, p. 026003, 2013.
- [25] A. D. Marchese, C. D. Onal, and D. Rus, "Soft robot actuators using energy-efficient valves controlled by electropermanent magnets," in *Intelligent Robots and Systems (IROS), 2011 IEEE/RSJ International Conference on*. IEEE, 2011, pp. 756–761.
- [26] R. F. Shepherd, F. Ilievski, W. Choi, S. A. Morin, A. A. Stokes, A. D. Mazzeo, X. Chen, M. Wang, and G. M. Whitesides, "Multigait soft robot," *Proceedings of the National Academy of Sciences*, vol. 108, no. 51, pp. 20400–20403, 2011.
- [27] R. F. Shepherd, A. A. Stokes, J. Freake, J. Barber, P. W. Snyder, A. D. Mazzeo, L. Cademartiri, S. A. Morin, and G. M. Whitesides, "Using explosions to power a soft robot," *Angewandte Chemie*, vol. 125, no. 10, pp. 2964–2968, 2013.